Review Article

JCBFM

Journal of Cerebral Blood Flow & Metabolism
2018, Vol. 38(9) 1500–1516

DOI: 10.1177/0271678X17700913
journals.sagepub.com/home/jcbfm
SAGE

Imaging the physiological evolution of the ischemic penumbra in acute ischemic stroke

Richard Leigh[1], Linda Knutsson[2,3], Jinyuan Zhou[3,4] and Peter CM van Zijl[3,4]

Abstract

We review the hemodynamic, metabolic and cellular parameters affected during early ischemia and their changes as a function of approximate cerebral blood flow (*CBF*) thresholds. These parameters underlie the current practical definition of an ischemic penumbra, namely metabolically affected but still viable brain tissue. Such tissue is at risk of infarction under continuing conditions of reduced *CBF*, but can be rescued through timely intervention. This definition will be useful in clinical diagnosis only if imaging techniques exist that can rapidly, and with sufficient accuracy, visualize the existence of a mismatch between such a metabolically affected area and regions that have suffered cell depolarization. Unfortunately, clinical data show that defining the outer boundary of the penumbra based solely on perfusion-related thresholds may not be sufficiently accurate. Also, thresholds for CBF and cerebral blood volume (*CBV*) differ for white and gray matter and evolve with time for both inner and outer penumbral boundaries. As such, practical penumbral imaging would involve parameters in which the physiology is immediately displayed in a manner independent of baseline *CBF* or *CBF* threshold, namely *pH*, oxygen extraction fraction (*OEF*), diffusion constant and mean transit time (*MTT*). Suitable imaging technologies will need to meet this requirement in a 10–20 min exam.

Keywords

Acidosis, ischemic penumbra, metabolism, MRI, perfusion, pH, physiologic evolution

Received 10 December 2016; Revised 30 January 2017; Accepted 27 February 2017

Acute ischemic stroke treatment and diagnostic needs

The treatment of acute ischemic stroke has historically been performed with incomplete image guidance. Although non-contrast computed tomography (CT) is commonly used to exclude hemorrhagic stroke prior to administering intravenous tissue plasminogen activator (tPA) and has some potential to visualize irreversibly damaged tissue during early ischemia (hypodensity and loss of gray/white matter contrast characterized by the Alberta Stroke Program Early CT score (ASPECTS)[1]), it is currently not providing any immediate information regarding changes in physiological tissue status related to pH, metabolism, and acute cell depolarization. While such a "blind" approach has been partially successful due to a heavy reliance on speed of treatment,[2] the focus on delivering tPA ever more quickly is a strategy of diminishing returns. While the mantra "time is brain" may be an important rallying cry for those developing systems for delivery of care, it is an oversimplification that has the potential to obscure our understanding of the pathophysiology we aim to treat. Most patients presenting with acute stroke are

[1]National Institute of Neurological Disorders and Stroke, National Institutes of Health, Bethesda, USA
[2]Department of Medical Radiation Physics, Lund University, Lund, Sweden
[3]Department of Radiology, Johns Hopkins University, Baltimore, MD, USA
[4]F.M. Kirby Center for Functional Brain Imaging, Kennedy Krieger Institute, Baltimore, MD, USA

Corresponding author:
Peter CM van Zijl, Department of Radiology, Division of MRI Research, School of Medicine, Johns Hopkins University, 217 Traylor Building, 720 Rutland Avenue, Baltimore, MD 21205-2195, USA.
Email: pvanzijl@mri.jhu.edu

ineligible for treatment when triaged using the time-based model. For instance, in the US less than 10% of stroke patients presenting to the hospital are treated with IV tPA.[3] The majority of patients who go untreated are not offered acute therapy because they do not fit into this time-based model.[4] Endovascular therapy has greatly improved the efficacy of intravenous tPA for patients with a large vessel occlusion.[5–8] Unfortunately, currently even fewer stroke patients are candidates for the combined treatment, e.g. 1% of screened patients in a recent clinical trial,[7] also in part due to this being a time-based therapy.[9] Still, this number will increase in the next decade and these are the 1% most severe stroke patients (occluded middle cerebral artery). Approximately 800,000 people suffer a stroke in the US yearly.[10] Thus, there is a large population of stroke patients who are not being evaluated for treatment due to the widely used time-based model for selecting patients for therapy. It will always be crucial for acute stroke interventions to be delivered rapidly and it has been clearly demonstrated that advanced imaging is generally not needed to treat patients who present in an early time window. However, for patients that are excluded from treatment due to time restrictions or in which treatment application is indicated but uncertain due to lack of knowledge regarding tissue already progressing to infarction, there is an opportunity for advanced physiologic imaging to expand the treatable population. The number of additional patients that may benefit from such physiologic imaging is currently unknown and has to be evaluated in future trials. Advanced imaging may also be useful to evaluate the success of treatment in terms of physiological recovery and for assessing the effect of neuroprotective approaches.

MRI and PET studies (for some reviews with references, see literature[11–17]) have demonstrated the presence of viable tissue in stroke patients at time points as far out as 24 h post-onset of symptoms, and spuriously even up to 48 h. In addition, the results of the MR WITNESS trial, which were recently presented at the 2016 International Stroke Conference in Los Angeles, suggested that MRI could be used to safely administer tPA to patients who had an unknown time of onset. Clearly, there is a great opportunity for improving stroke outcomes if imaging methodologies are available that can, in a timely fashion, evaluate the physiological and hemodynamic status of the tissue allowing a more educated decision regarding treatment. From a practical point of view, this would require four key points: (i) exclusion of hemorrhage, (ii) assessment of patency of the main perfusing arteries, (iii) differentiation of viable tissue at risk of progressing to infarction from tissue that is destined for infarction, and (iv) identification of tissue that is already infarcted. While the first two goals can be achieved readily with CT, or MRI, the third requirement is more complicated. Fortunately, decades of basic research have elucidated the dependent nature of tissue metabolism on cerebral blood flow (*CBF*) thresholds and established great insight into the parameters needed to make such an assessment of tissue viability. While not the objective of this review, it is important to point out that identification of infarcted tissue has potential for risk assessment for treatment complications such as hemorrhagic transformation.[18,19] Thus, combining physiologic imaging with markers of complication risk may ultimately be the best approach for patient selection.

The current scientific philosophy for assessment of tissue viability (point (iii)) is to use the existence of an evolving ischemic penumbra as the criterion for possible reperfusion treatment. This concept originates from baboon studies in which manipulation of the *CBF* was used to identify thresholds of cerebral ischemia.[20] The penumbra was originally described in terms of a brain region of cerebral dysfunction due to electrical failure[20,21] but with cellular energy sufficient to maintain a cell membrane potential. However, it has become generalized to describe regions affected by ischemia that are at risk of infarction, but reversible with timely restoration of *CBF*.[22–24] Modern imaging methods can identify such a penumbra by measuring multiple physiological parameters that change during ischemia with changing *CBF*. Therefore, before discussing the "most suitable" penumbra and deliberating which imaging parameter may best describe this penumbra, it is first necessary to summarize the dependence of tissue metabolism on *CBF* thresholds and review which imaging technologies can assess the physiologic evolution of ischemic tissue in a way that is accurate and, more importantly, quick and comprehensive.

Ischemic thresholds and the physiological evolution of hypoperfused tissue

Figure 1 summarizes approximate *CBF* thresholds for a multitude of physiological changes in ischemic tissue. The *CBF* values are based on PET studies in humans (see earlier works[12,16,25] and references therein) assuming a normal gray matter *CBF* of 50 ml/100 g/min and keeping in mind that these thresholds may differ between species[12,23,26] as well as between tissues with different metabolic demands, such as gray and white matter. Additionally, different imaging technologies may yield different *CBF* numbers, e.g. while MRI values may tend to be high because of partial volume effects with arteries being more important than with white matter, PET may yield lower values due to partial volume effects with white matter. A more general

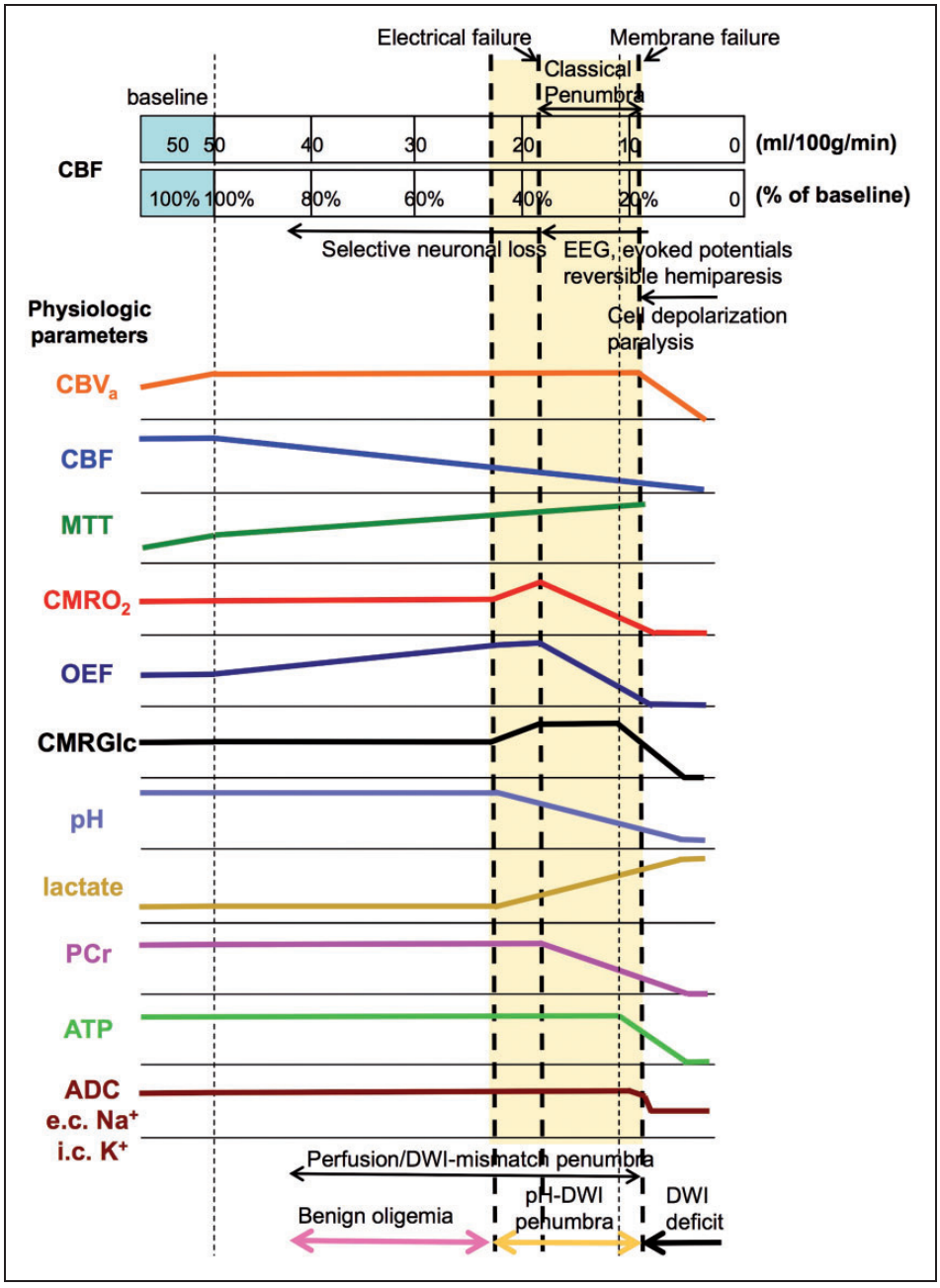

Figure 1. Relationships between CBF thresholds (human) and neurological, hemodynamic, metabolic, and cellular parameter changes. Thresholds are approximate, assuming PET-based normal gray matter CBF of about 50 ml/100 g/min, and may shift to higher CBF with longer ischemic duration. Curve can be adjusted proportionally for baseline CBF from other methods, such as MRI and CT. Curve heights are relative to baseline on the left. The blue extended area at constant CBF of 50 ml/100 g/min is needed to depict the area of autoregulation during initial vessel blockage and reduction in cerebral perfusion pressure where CBV increases and flow remains constant. Metabolic penumbra in yellow shade. At the bottom, zones of perfusion-DWI and pH-DWI mismatch are shown, with the difference being benign oligemia. Color coding for these zones will be used in Figure 3.
e.c: extracellular; i.c: intracellular.

approach would therefore be to show percentage of baseline flow, which has been added to this graph too ($\%\text{threshold} = 100\% \times PETCBF/50$). Furthermore, these thresholds should be considered as lower boundary as they will evolve over time[27] and may also have a rate of change that varies between individuals. As such, it is important to recognize that imaging provides only a single time-constrained view and that treatment decisions and consequent actions should be taken as soon as possible thereafter. Additionally, due to the inherent

range of relevant flow levels and variation in thresholds between different tissue types, measurement of absolute *CBF* in acute stroke is expected to be less informative than direct measurement of molecular changes or physiologic parameters consequent to metabolism, e.g. *pH*. Hossmann[23] captured this sentiment saying,

> injury in the periphery of the ischemic infarct is not solely a function of the rate of blood flow……the understanding of the pathophysiology of penumbra has to consider both the reduction of blood supply and the state of functional activation.

When a large feeding arterial vessel is blocked, a drop in cerebral perfusion pressure (*CPP*) occurs. In an effort to keep *CBF* constant, autoregulation causes cerebrovascular resistance (*CVR*) to reduce proportionally to *CPP*[28] through dilatation of post-arterial and arteriolar vessels with smooth muscle cells and of the pericytes in the capillaries.[29,30]

$$CBF = CPP/CVR \tag{1}$$

This leads to an increase in arterial + arteriolar cerebral blood volume (CBV_a) and total *CBV*. The constant flow and increased volume are reflected in an early increase in the mean transit time (*MTT*) retrieved using the central volume theorem[31]

$$MTT = CBV/CBF \tag{2}$$

If the blockage remains and the compensatory vasodilation is insufficient, *CBF* will ultimately decrease, leading to a cascade of molecular events and selective neuronal loss,[32] the extent of which depend on the level of the residual flow. The first requirement is to maintain the cerebral metabolic rate of oxygen ($CMRO_2$), which can be accomplished temporarily by increasing the oxygen extraction fraction (*OEF*) from blood. This parameter can be calculated from the ratio of oxygen consumption and delivery

$$OEF = CMRO_2/(C_a \cdot CBF) \tag{3}$$

where C_a is the oxygen content, the product of the arterial oxygenation fraction ($Y_a = \frac{S_{aO2}}{100\ \%}$) and hemoglobin concentration, which is proportional to the hematocrit fraction (*Hct*). Oligemia can be defined to cover regions where the flow reduction is balanced by increased oxygen extraction from the blood to maintain $CMRO_2$. Interestingly, when the flow keeps dropping further to about 40–45% of baseline,[33] the cerebral metabolic rate of glucose (*CMRGlc*) first increases. Two explanations have been put forward for this,[33] the first being the occurrence of spreading depression like depolarizations (which would also increase $CMRO_2$), the second is that there is an increase in anaerobic metabolism to maintain ATP levels. To indicate these phenomena in Figure 1, we show an increase in both $CMRO_2$ and lactate for this flow range, together with a *pH* drop, but ultimately it may be that only one of the two mechanisms applies. The occurrence of spreading depression would lead to release of glutamate, and the fact that glutamate antagonists are protective gives some support to this interpretation. However, the two phenomena are not mutually exclusive and probably occur together.

Once *CBF* levels drop further to the threshold at which maximal oxygen extraction is reached, subsequent decreases in *CBF* force upon the brain tissue a proportional reduction in oxygen consumption, concomitant with a further increase in lactate and reduction in *pH*. Below this *CBF* threshold of about 35–40% of baseline, loss of tissue function occurs that can be detected as incapacitation of electrical activity. A continued decrease in *CBF* results in more severe hypoxia and a further increase in in lactate and lowering of *pH*. In addition, phosphocreatine (PCr) levels start to drop.[34–36] Eventually, at a threshold of about 20–24% of baseline, glucose utilization and ATP levels drop rapidly leading to a massive release of intracellular potassium and anoxic membrane depolarization with intracellular accumulation of Na^+ and water (cytotoxic edema).[37] Without timely revascularization (either spontaneous or with treatment), this situation leads to vessel collapse, a consequent reduction of *CBV* to zero, and ultimately to irreversible tissue damage. In Figure 2, an in vivo illustration of the events displayed in Figure 1 is given for 4-vessel occlusion in the rat brain, showing reversibility for PCr, lactate, *pH* and *OEF* (BOLD effect, explained below) in case of timely reperfusion, while ATP and some of the field potentials do not totally recover.[38]

The important fundamental studies above led to the two threshold model of cerebral ischemia in which reduction in *CBF* up to a first threshold of EEG amplitude reduction represented oligemia, while reduction up to a second threshold yielded reversible cerebral dysfunction, beyond which there is loss of structural integrity and irreversible infarction.[39] The spatial pattern of these regions in the setting of a large artery occlusion, in which the region of reversible ischemia surrounds the region of irreversible infarct, led to the designation of the ischemic penumbra.[21] Thus, penumbra was initially defined as the region with electrical failure (neuronal dysfunction) but not cellular energy failure (structural loss), indicated as ''classical penumbra'' in Figure 1. While subsequent studies looking at the molecular changes associated with cerebral ischemia have found this model to be an oversimplification,[23] it became the

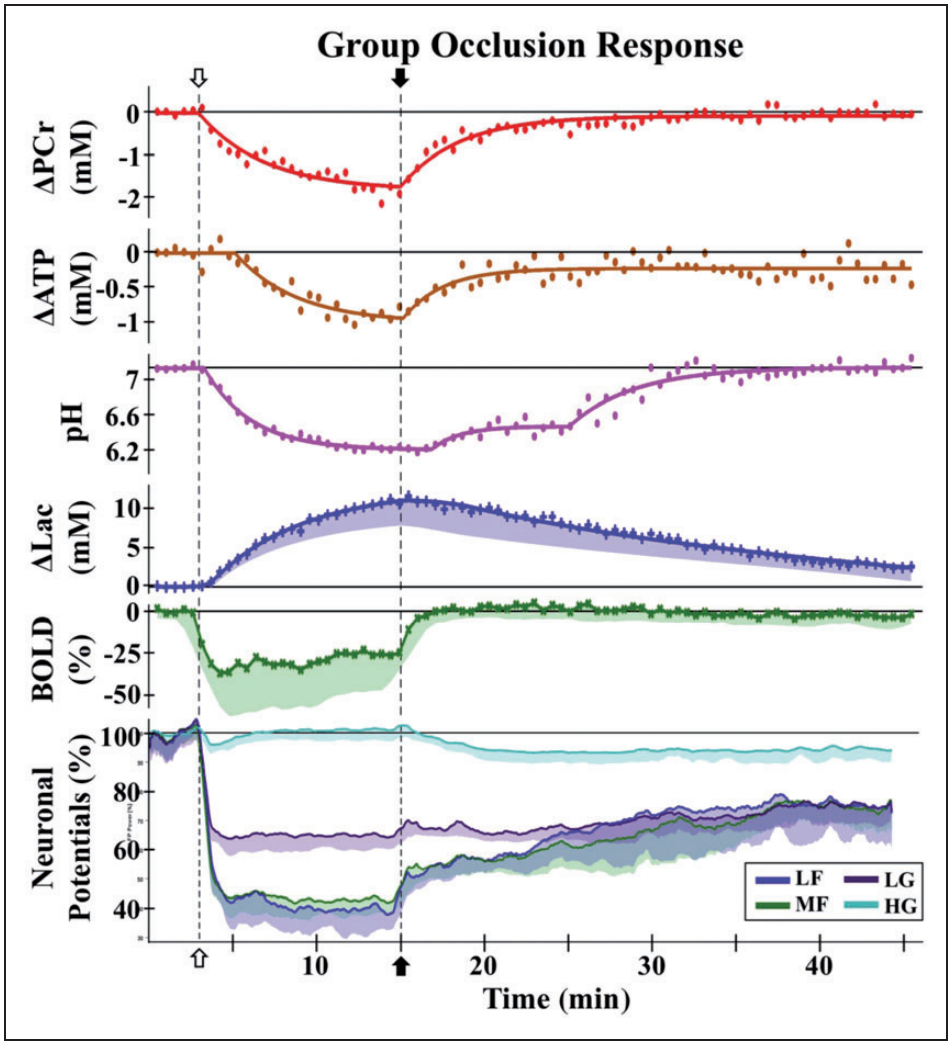

Figure 2. Physiological MRI responses and neuronal potentials as a function of time after reversible occlusion (12 min) of both common carotid arteries in rats with previously cauterized vertebral arteries. Group responses to occlusion (open arrow) and reperfusion (filled arrow) with raw data (symbols) and regression fits (lines) for ΔPCr, ΔATP, pH, and Δlac, ΔBOLD (raw data), and neuronal field potential activity (smoothed data lines). Average of individual animal values, with shaded areas indicating one standard deviation (σ) from the mean. Field potentials were analyzed across four frequency bands: low frequency (LF), 0–10 Hz; medium frequency (MF), 10–30 Hz; low gamma (LG), 30–58 Hz; high gamma (HG), 62–200 Hz. Neither ATP nor field potential bands recover to baseline levels.

ATP: adenosine triphosphate; BOLD: blood oxygenation level dependence; Lac: lactate; PCr: phosphocreatine (Reproduced in part, with permission, from Taylor JM, et al. *NMR Biomed* 2015; 28: 1357–1365.)

clinical model guiding stroke management. Over time, it was recognized that the penumbra pattern was time dependent.[40,41] This shifted the description of penumbra from a region of a certain type of tissue dysfunction to the more practical one of potential tissue salvage. The penumbra came to be defined as tissue that was doomed to infarction in the absence of early reperfusion. The idea that the ischemic penumbra is the target of reperfusion therapies has been the driving force behind acute stroke research ever since. In addition, the necessity to properly assess the presence of a penumbra has stimulated the development of imaging approaches to display such tissue at risk.

Visualizing a penumbra

Current imaging technologies that can visualize some of the parameters in Figure 1 are summarized in Table 1. The goal of this review, however, is not to provide an in-depth explanation or review of such technologies, but to, based on considerations of physiological relevance (Figure 1) and practicality in the clinic, analyze

Table 1. The three major imaging methods for acute stroke and parameters they can detect*,**.

Physiologic Parameter	PET	CT	MRI
Hemorrhage		Hyperdense	**T_2* hypo-intensity,[130] SWI,[130] APT[131]**
Site of occlusion		CTA	**MRA**
destined for infarction (Neuronal death)	^{11}C-FMZ ^{18}F-BCPP-EF	Hypodense	**T_2 hyper-intensity**
CBV	$^{15}O_2$	CTP	**DSC, VASO (mainly GM)[132]**
CBV_a			**iVASO (mainly GM)[133]**
CBF	$^{15}O_2$	XeCT/CTP	**DSC, ASL (mainly GM)[134]**
MTT	$^{15}O_2$	CTP	**DSC**
$CMRO_2$	$^{15}O_2$		**QSM,** indirectly by ^{13}C MRS, MRI
OEF increase	$^{15}O_2$		**QSM,** **T_2 and T_2* mild hypo-intensity**
CMRGlc	^{18}FDG		^{13}C MRS
Hypoxia	^{18}F-MISO		**BOLD (T_2, T_2*)**
Lactate			**^{1}H MRS**, ^{13}C MRS
pH	$^{11}CO_2$, ^{11}C-DMO		^{31}P MRS, **CEST/APT MRI**
PCr/Cr			^{31}P MRS, **CEST MRI[128]**
ATP			^{31}P MRS
Na			^{23}Na MRI
ADC			**DWI, DTI**

*MRI methods possible on standard clinical scanners are in BOLD. **Most citations are in the text; only references for clinically accessible methods not mentioned in the text are added to the table.

FMZ: flumazenil; ^{18}F-BCPP-EF: 2-tert-butyl-4-chloro-5-{6-[2-(2-(18)F-fluoroethoxy)-ethoxy]-pyridin-3-ylmethoxy}-2H-pyridazin-3-one; FDG: Fluorodeoxyglucose; MISO: misonidazole; DMO: dimethyloxazolidinedione; CTA: CT angiography; CTP: CT perfusion; SWI: Susceptibility-weighted imaging; CEST: Chemical exchange saturation transfer; APT: Amide proton transfer; MRA: Magnetic resonance angiography; DSC: Dynamic susceptibility contrast; VASO: Vascular space occupancy; iVASO: inflow VASO; ASL: Arterial spin labeling; QSM: Quantitative susceptibility mapping; MRS: MR spectroscopy; DWI: Diffusion weighted imaging; DTI: Diffusion tensor imaging.

current and potential approaches to identify a future strategy for a fast clinical scan that captures just the information needed to address points (i) – (iv) summarized above. In this respect, when reading the literature,[16,17,23,25] a consensus is clear that the most practical penumbral outer boundary for making decisions would be one that identifies the regions of hypoxia for which early changes in glucose metabolism have shifted from aerobic to anaerobic resulting in a concomitant increase in lactate with a reduction in *pH*. The inner boundary would occur at the point of irreversible cell depolarization. In his early review in 1994, Hossmann[23] states: ''Consequently, the penumbra can be imaged by subtracting the ATP lesion from the *pH* lesion.'' We believe that imaging a penumbra based on this practical definition that excludes benign oligemia is the most relevant goal and adopt this definition whenever referring to a penumbra in the discussion below.

Further requirements for imaging parameters in terms of fast clinical decisions relate to the practicality of such an exam. First of all, to include as many hospitals as possible, standard readily accessible equipment should be used. Unfortunately, this almost always rules out PET and SPECT and leaves CT and MRI for default use. However, even MRI is often hard to access in a timely manner, despite being commonly available in modern hospitals. Furthermore, advanced MR approaches using heteronuclei are most often not available and even MR spectroscopy (MRS) will be too time consuming. We therefore, in Table 1, highlighted in bold letters only those approaches that are proton (^{1}H) imaging based. If our goal is to have a 10–20 min exam with immediate multi-dimensional (3D or multi-slice whole brain) results regarding tissue physiology, it would be most useful to have straightforward images that provide the required information for both gray matter and white matter. As such, the use of quantitative *CBF* thresholds seems cumbersome for the clinician in view of the existence of differences in flow thresholds between these tissues, particularly given the time dependence of the physiological processes. Examples of such tissue and time independent methods could be imaging of hypoxic markers, methods to image lactate and *pH* for visualizing the consequences of anaerobic metabolism, and parameters such as *MTT* and *OEF*, where the difference between gray and white matter is removed due to division of proportional quantities, i.e. *CBV* and *CBF* in *MTT* (equation (2)) and $CMRO_2$ and

CBF in *OEF* (equation (3)). Just as an illustration, while gray matter has been found to be at risk around *CBF* 20 ml/100 g/min, this is 12.3 ml/100 g/min for white matter.[42,43] However, the *MTT* threshold has been found to be the same at 6.8 and 7.1 s.[42,43] While ischemia removes the physiological coupling between *CBV*, *CBF*, and $CMRO_2$, for *OEF* and *MTT*, the contrast between gray and white matter in the normal tissue is absent, thus changes can be more easily visualized. Another parameter that is comparable in magnitude between gray and white matter is the trace of the diffusion tensor,[44,45] better known as the mean diffusivity, average apparent diffusion constant (ADC_{ave}) or isotropic *ADC*. Reductions in this parameter during spreading depression[46] and (much larger) after cell depolarization[47] can be accessed with isotropic diffusion weighted imaging (DWI). Finally, it always has to be realized that the inner and outer boundaries of the penumbra evolve and each imaging is just a representation of tissue physiology at a particular point in time.[40]

The inner boundary of the ischemic penumbra

The depiction of an area of irreversible tissue damage that is infarcted or will proceed to infarction is crucial in the concept of penumbral imaging. While infarcted tissue (point (iv) above) is easy to detect with MRI through T_2-hyperintensity in T_2-weighted or FLAIR images, T_2 is generally unchanged in early ischemia or even slightly reduced during hypoxia/ischemia (the inverse of the BOLD effect in functional MRI).[48,49] Availability of a method to detect the extent of irreversible neuronal damage in the acute phase is crucial to avoid unnecessary and potentially dangerous treatment using tPA. A suitable PET marker for neuronal integrity is ^{11}C-flumazenil (FMZ),[50] for which reduction in its binding below a certain threshold is a good indicator of damage. With respect to MRI, two decades of human research has indicated that hyperintense regions on diffusion weighted imaging (DWI) are mostly a marker of tissue destined to infarction. However, the DWI lesion is not totally accurate for such a prediction and it is now well realized that it can be reversible with reperfusion.[51–56] Of course, this is not surprising in view of the results from early animal studies, from which it was initially thought that DWI showed the outer penumbral edge.[27,57]

Historically, Moseley et al.[58] discovered in cats that hyperintensity on DWI, corresponding to a reduction in *ADC*, could identify acutely ischemic tissue, a breakthrough finding that was quickly replicated in humans.[59] Early work utilized directional diffusion weighting, which led to confusion regarding infarct progression. It was soon determined that trace-based DWI, which has minimal dependence on the underlying structure of the tissue, could more clearly delineate ischemic regions due to lack of contrast between gray and white matter. Trace DWI also allowed reproducible calculation of an absolute apparent diffusion coefficient (*ADC*)[44,45] which would later play an important role in establishing relevant thresholds.[60] Although directional DWI is commonly used for diffusion tensor imaging, "trace DWI," also called "isotropic DWI," is now the standard clinical tool for assessing acute stroke. Restriction of water movement detected with DWI was determined to represent a shift of water intracellularly due to failure of ATPase dependent ion pumps (Figure 1).[61] These changes were found to be rapidly reversible in the setting of reperfusion,[62,63] and the more recent human results are just a clinical confirmation of this. The reversal of DWI lesions in patients may be in part transient, and some investigators have reported there is no corresponding benefit.[64,65] However, others have reported transient lesion reversal may reflect clinical improvement.[51,52] The NIH stroke team, which routinely performs MRI before, and two hours after treatment of acute stroke patients enrolled in the NIH Natural History of Stroke study, regularly identifies reversal of DWI lesions. In a series of 58 stroke patients seen by the NIH stroke team, a decrease in stroke volume, based on an apparent diffusion coefficient threshold of 600, was seen in 57% of patients 2 h after treatment. A decrease in stroke volume was associated with significant improvement in NIHSS 24 h after the stroke ($p = 0.03$) even though 80% of the patients had recurrence of the lesions with median growth of 38%. These types of observations, which are in agreement with previous studies, call into question the role of DWI in delineating the ischemic penumbra. These findings are, however, consistent with our understanding of the evolution of the physiologically active ischemic penumbra described previously.

The outer boundary of the ischemic penumbra

The existence of a penumbra in humans was first identified with PET using $^{15}O_2$ inhalation (which can also be combined with $H_2{}^{15}O$ injection to achieve steady state).[22,66] This methodology utilized combined measures of *OEF* and *CBF* to determine $CMRO_2$ and was able to identify areas of misery perfusion (reduced *CBF*, increased *OEF*) and persistent $CMRO_2$. Looking at Figure 1, this PET-based definition[12] would include benign oligemia with all levels of hypoxia and be less accurate in predicting a region immediately at risk. However, the reported gray matter *CBF* thresholds (~20 ml/100 g/min) from the latter paper typically correspond to regions of severe hypoxia or may indicate that the sensitivity of PET toward detecting changes in *OEF* is close to this level of hypoxia.

Later work by Guadagno et al.[67] confirms that a proper definition of a penumbra for assessment of risk is one with an outer rim encompassing regions of hypoxia. Heiss[16] indicates that "a biochemical marker of core plus penumbra is tissue acidosis." Thus, good targets for visualizing the outer rim are parameters reflecting tissue hypoxia or anaerobic metabolism (lactate and *pH*) or certain *OEF* and *MTT* thresholds that would correspond to areas of tissue hypoxia or acidosis. We briefly discuss the possibility to image perfusion and tissue hypoxia and acidosis using PET, CT and MRI.

Outer-boundary-perfusion-based

Since the penumbral concept is based on *CBF* thresholds, it is useful for stroke exams to include perfusion measures to get insight into the existence of viable low-flow regions. Perfusion imaging can be done fast and reliably using dynamic perfusion CT (PCT)[68] and dynamic susceptibility contrast (DSC) MRI.[69–73] Both methods are similar in that a tracer is injected (Table 1) and regional differences in delivery can be visualized. While many patient assessments only depict the presence of a perfusion deficit, more quantitative information can also be obtained. Using the arterial input function (AIF) from a suitable artery to deconvolve the tissue concentration time curve, the tissue "residue function," describing the retention of a tracer in the tissue, can be determined and subsequently be used to estimate *CBF*. In addition, *CBV* can be obtained by taking the integral of the tissue concentration time curve and normalizing it to the integral of the arterial input function. More importantly, these measures can be used to calculate the *MTT*[74] (equation (2)), which is less tissue (gray/white matter) dependent and can be used to identify ischemic tissue on a homogeneous looking image.[68,71,75]

Over the past two decades, assessment of the ischemic penumbra with MRI has used DSC-based perfusion-weighted imaging (PWI) to identify its outer edge[76] and DWI to identify its inner edge. Although this DWI-PWI mismatch has become a widely-used biomarker for estimating the ischemic penumbra, its validity has been controversial. We saw above that the DWI lesion does not always signify irreversible infarct, but, more relevant, the concept that the PWI lesion represents tissue at risk is often flawed. The term benign oligemia was put forth to describe regions of decreased blood flow that do not progress to infarction and their inclusion within the PWI-DWI mismatch was thought to be a confounding factor in several early trials.[77,78] To improve this situation, real time on-scanner post-processing to quantify *CBV, CBF* and *MTT* has been proposed;[79,80] however, this is difficult to do accurately,[81,82] introduces additional variability,[83,84] and has a performance that is not better than with simpler methods.[85] The time to maximum of the peak of the residue function (*Tmax*) was subsequently used as a PWI parameter in acute stroke.[86] While *Tmax*, at a threshold of >6 seconds, has shown to be an improved measure of the penumbra in clinical trials,[65,77,78,87] it is not routinely generated by clinical scanners or off-line software packages and, alternatively, the measure of time to peak (*TTP*) of the tissue concentration time curve is commonly used in practice as a replacement. However, *TTP* is not based on the residue function and cannot be used reliably as a replacement for Tmax. These two parameters also need not be linearly proportional, and the use of different thresholds and injudicious substitution between these parameters can be confusing for the clinical team that needs to make a timely decision. More recently, different on and off-scanner processing software packages that automatically generates Tmax maps have become commercially available. This adds to the difficulty comparing between sites and a consensus is needed to standardize measures. The approach used to address this issue for the multi-center clinical trial DEFUSE 3 is to use a single vendor across all sites. The downside of this approach is that it ties the results of the trial to a commercial entity.

In clinical practice, when trying to image the ischemic penumbra, PCT is often substituted for MRI. While initially limited to partial brain coverage, which is no longer an issue with newer scanners, it also has the great conveniences of speed and universal access. For PCT, DWI is not available and the inner threshold was originally approximated with a *CBV* cutoff value,[88] and subsequently with a *CBF* threshold,[89] but more recently with a dual *MTT-CBF* based cutoff.[90] Studies have shown a reasonable match between PCT and DSC-PWI penumbral volumes[91] and sometimes, when using the same off-line processing software, even *Tmax*.[92] However, such an agreement can also often be achieved by judicious choice of thresholds within one laboratory. Unfortunately, different CT companies often have their own PCT software that can lead to substantial variability in the resulting *CBF, CBV* and *MTT* numbers, and thus the corresponding threshold based penumbra.[90,93] This lack of standardization will greatly hamper multi-site trials and the comparison with MRI. Another issue, similar for both quantitative PCT and PWI, is that the calculated parameters and resulting thresholds depend on the suitability of the AIF, which often is chosen in the contralateral hemisphere and thus not a true reflection of the actual AIF which should in principle be judged ipsilaterally. For instance, on many images in the clinic, *MTT* appears as very long in areas already infarcted, where *CBV* blood vessels are most likely collapsed and *CBV* expected to be zero. Thus, care has to be taken with its

interpretation, which is why we stopped the graph for *MTT* right after the depolarization threshold in Figure 1. Even if all hospitals would use a similar AIF approach and the same post-processing software, it would be hard to reach agreement about thresholds as partial volume effects will differ and affect the numbers measured. Therefore, the use of quantitative dynamic perfusion parameters is ultimately too complex and difficult to standardize between hospitals. Additionally, the penumbra is always evolving and the time of imaging post-onset or the severity of the occlusion may vary greatly, which makes thresholds of flow and volume and even *MTT* less meaningful in terms of molecular consequences.

Outer-boundary-oxygenation-based

HYPOXIA-USING-PET

More recent PET methodologies have been able to identify what originally was thought to be a predominantly hypoxic penumbra using the freely diffusible tracer ^{18}F-fluoromisonidazole (^{18}FMISO).[94–97] Experimental studies in animals initially indicated that FMISO specifically detects severely hypoxic tissue that is still viable, but not benign oligemia nor the ischemic core. (Takasawa et al.[98] and references therein). In addition, data were comparable but not equivalent for gray and white matter. When using ^{18}FMISO in humans, large regions of hypoxic tissue surrounding the ischemic core could be found as long as 48 h after symptom onset,[99] a large part of which reverted spontaneously back to normal. Such data indicate that the penumbra outlined this way may be an overestimate. Another limitation of this tracer is its slow kinetics, requiring about a 2-h wait before scanning after infusion. Thus, although PET imaging has many useful tracers for stroke which have been crucial in defining quantitative ischemic thresholds in humans[12,100] and for understanding the concept of an ischemic penumbra, its current clinical utility in acute stroke is unfortunately minimal due to the lack of availability and feasibility for performing a fast scan.

OEF-USING-MRI

Several attempts are being made to develop more direct MRI measures of cellular status such as *OEF* (and $CMRO_2$ calculated from *OEF*) and *pH*, reflecting continuing cellular activity and the physiological consequence of anaerobic metabolism, respectively. Actually, it is often not realized that *OEF* is a parameter studied frequently by MRI, as changes in *OEF* are the main cause underlying the BOLD effect, where a local increase in *CBF* decreases *OEF*. This is reflected in an increase in capillary and venous oxygenation fraction ($Y_v = \frac{S_{vO2}}{100\ \%}$) and an increase in the relaxation times T_2 and T_2*. For an arterial blockage, the situation is opposite (*OEF* increases and Y_v reduces) and even the arterial oxygenation fraction (Y_a) reduces post-blockage, causing a larger increase in *OEF* (equation (3)). The rates $1/T_2$ and $1/T_2$* of blood are inversely related to the deoxygenation fraction (1-*Y*) in a vessel. For the venous oxygenation fraction in the case of hypoxia, it has been derived that:[49]

$$1 - \mathrm{Y_v} = 1 - \mathrm{Y_a} + \mathrm{OEF} \cdot \mathrm{Y_a} \quad (4)$$

Thus, a decrease in Y_a and increase in *OEF* (proportionally larger than the decrease in Y_a) will decrease the venous oxygenation and lower T_2 and T_2*. Measurement of these relaxation times in the veins can be used to determine *OEF*.[101–104] These changes in oxygenation affect the magnetic susceptibility in and around the vessels and such a decrease in oxygenation will darken absolute T_2 and T_2* images. Note that this is the effect used to image hemorrhage with MRI. Similarly, susceptibility-weighted imaging (SWI) can display these changes and quantitative susceptibility mapping (QSM) can also be used to determine vessel oxygenation related to these changes and thus *OEF*.[105–109] If *CBF* is determined in addition, T_2, T_2* or susceptibility data can also be used to estimate $CMRO_2$ by using equation (3) and the oxygen content. However, these parameter determinations are for large draining vessels, which is fine for whole-brain studies but not for stroke, where physiological changes are local. An and Lin[110–112] showed that the extravascular effects of changes in blood oxygenation can be used for more local *OEF* and oxygen metabolism estimates, using the BOLD theory of Yablonskiy and Haacke.[113] For metabolism, they used the product of *OEF* and *CBF* to derive the parameter MR_COMI (cerebral oxygen metabolic index)[112] or MR_OMI.[114] The BOLD theory requires knowledge of the venous *CBV*, which can be estimated from DSC-MRI. However, determining local *OEF* and oxygen metabolism is still complicated in the case of ischemic stroke, because the AIF used to quantify *CBV* and *CBF* from DSC-MRI is generally not taken from the blocked artery (post-clot) but a close by or contralateral artery. However, these parameters, while not fully quantitative in the case of very acute stroke, may still be very useful to display the area at risk of progression to infarction and recently some promising examples of this could be demonstrated for the parameter *MR_OMI*. [114] However, the *OEF* and thus the *MR_COMI* may overestimate this region, similar to *CBF* (Figure 1). It then becomes a matter of appropriate thresholding to estimate the penumbra within the

total zone. Finally, when the stroke progresses, the relaxation times increase due to edema, so the interpretation of T_2 and T_2* for the purpose of determining *OEF* will become more difficult.

PH-USING-MRI

Due to the potential for clearly outlining areas of anaerobic metabolism, and thus the ischemic penumbra, there has been great interest in developing a *pH*-weighted or lactate imaging MR pulse sequence. While MRS has had the capability of quantifying *pH* using the phosphorus (^{31}P) nucleus,[35] this approach is not practical for acute stroke clinics due to poor sensitivity and limited availability. Lactate visualization using so-called spectroscopic imaging has been demonstrated,[115] but again not currently very practical in view of limited brain coverage and lengthy setup and acquisition times (at least 20 min). Another study showed that the effect of *pH* could be measured on the signal intensity of the exchangeable amide protons of cellular proteins and peptides in the proton spectrum.[116] Since the exchange rate of such protons is *pH*-dependent,[117] measurement of this exchange would enable *pH* imaging. However, similar to lactate, amide proton MRS is limited by poor special resolution and long acquisition times. Fortunately, the advent of a technique called chemical exchange saturation transfer (CEST) imaging[118,119] has made it possible to detect low-concentration exchangeable protons indirectly through their exchange interaction with the water protons, resulting in greatly enhanced sensitivity (two or more orders of magnitude). This has given rise to the endogenous mobile protein and peptide-based technique named amide proton transfer weighted (APTw) MRI,[120] which is a safe, completely non-invasive technology using standard proton MRI equipment and thus readily translatable to the clinic.

The possibility of imaging *pH* with APT MRI was first demonstrated in a global ischemic model and in a permanent middle cerebral artery occlusion (MCAO) model in the rat brain.[120] Notably, in this study, the change in amide proton transfer ratio (APTR) as a function of tissue *pH* was calibrated, using ^{31}P spectroscopy for *pH* assessment, and an absolute *pH* map was then generated. Following this initial study, the capability of using the APT approach to detect a separate *pH*-based acidosis penumbra was further investigated.[121,122] Adult rats with permanent MCAO were imaged using multi-parametric MRI over the first 3.5 h post-occlusion. The endpoint was to visualize the stroke area defined by T_2 hyperintensity at 24 h. The images as a function of time post-occlusion in Figure 3(a) illustrate an example for one rat with limited occlusion, but still showing a clear perfusion deficit in which no diffusion lesion is visible in the *ADC* images even up to 3.5 h post-occlusion. Similarly, there is minimal contrast or contrast evolution on T_1 and T_2 images in this early period, but the observant viewer can see a T_2 reduction in the ipsilateral hemisphere, most likely corresponding to a BOLD effect due to increase in *OEF* as discussed above. A clear *pH* deficit is visible on all of the *pH*-weighted images. The follow-up scan at 24 h shows that ischemic evolution is still ongoing with an infarct outlined by T_2 and T_1 hyperintensity and clear changes in *ADC*. For the group of 18 rats, this study showed that the *pH* deficit correctly predicted the infarction, while the *ADC* region did not. This is summarized in the graph in Figure 3(b), where the vertical scale is area as percent of the *CBF* deficit, showing that the perfusion deficit overestimates the final lesion, while the *ADC* deficit underestimates it, in line with the principles of the penumbra outlined above. This principle is outlined schematically in Figure 3(c) and shown in Figure 3(d) for data analyzed on two more rats (color maps corresponding to Figure 3(c) code), where the *pH* area predicted the final infarct at 24 h. These data suggest that the hypoperfused area, showing a decrease in *pH* without an *ADC* abnormality, corresponds to the ischemic acidosis penumbra, while the hypoperfused region at normal *pH* corresponds to benign oligemia.

For APT-based pH imaging to take a place in the armory of acute stroke techniques, more studies are needed on validating the technology (e.g. using histology[123–125]). The use of histology to define a penumbra is difficult in the practical definition of outlining the outer boundary of a region at risk evolving to infarction, because performing pH histology would require killing of the animal without changing the physiology. While this can be approximated by rapid freezing, this may change the structural features and relative sizes of brain structures. In addition, cutting of the slices and coregistration and comparison with the much thicker brain slices remains a difficult issue. Furthermore, histological study of the temporal evolution of ischemia would require the use of many animals, for which the evolution may be different due to slight differences in individual physiology and experimental procedures. Most investigators therefore have used more indirect evaluations, such as the ultimate area of infarction as outlined by T_2w MRI,[121] which itself has been validated by staining. However, it ultimately is important to demonstrate that pH imaging outlines the correct area of pH change, for which histology should be used. In addition to validation, there is a need for studies assessing the appropriateness of using APT-based pH imaging for assessing pH evolution, e.g. following reperfusion or other types of treatment.

The implementation of this *pH* sensitive MRI technology on clinical scanners has been slow, mainly due to the small size of the APT effect and scanner

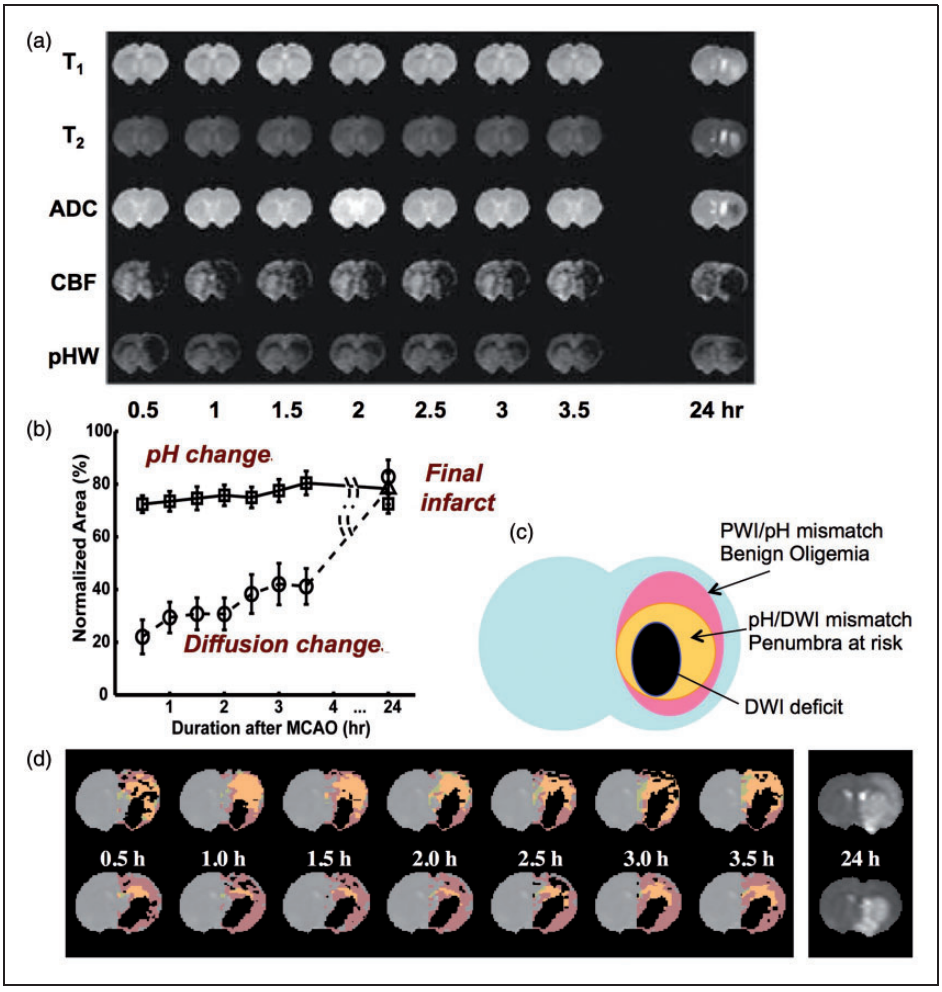

Figure 3. Multi-parameter MRI as a function of time after permanent MCA occlusion in rat. (a) Images of rat in which no T1, T2, and ADC changes were seen, but ischemia was confirmed by hemispheric CBF reduction (obtained using arterial spin labeling) as well as a pH-weighted deficit. Hyperintensity in the T2 image at 24 h gives the final infarction area. (b) Group analysis of ischemic volume evolution for 18 rats with perfusion/diffusion mismatch, comparing areas of pH change and diffusion change as fraction of the perfusion deficit region. The pHw region predicted well the evolution to infarction. (c) Parcellation of ischemic area in terms of three zones, a DWI deficit most likely proceeding to infarction, a pH/DWI mismatch region at risk of infarction and a PWI/pH mismatch not at risk. (d) Processed images for two other animals showing evolution of pHw-deficit (orange) and diffusion deficit (black) with respect to perfusion deficit (purple) as a function of time post-MCAO occlusion. The T2 image at 24 h shows final infarction area predicted well by diffusion + pHw regions. (Reproduced in part, with permission, from Sun PZ, et al. *J Cereb Blood Flow Metab* 2007; 27: 11–29).

hardware constraints. However, several groups have recently published initial clinical data suggesting that APT imaging is feasible for stroke patients and may provide extra information, by virtue of *pH* changes, about the infarct in ischemic strokes.[126,127] Very recently, Heo et al. (unpublished results in Figure 4) showed that the magnetization-transfer-asymmetry analysis approach commonly used is self-compensating in terms of subtracting *pH* effects and that focusing on just the signal change at the amide proton resonance can clearly outline *pH* deficits. Figure 4 shows some data from this recent work, which should make this approach more applicable in the clinic.

Considerations for a practical clinical acute stroke exam with detection of viable tissue at risk

As mentioned above, the main requirements for an optimum acute clinical stroke exam are speed (time is brain) and general availability of equipment with the ability to visualize hemorrhage, large vessel patency, the penumbra, and areas already infarcted or destined for infarction. This basically leaves CT and, to a lesser extent, MRI as the default methodologies, but future advances, such as PET-MRI potentially becoming commonly available may expand this. While CT beyond a

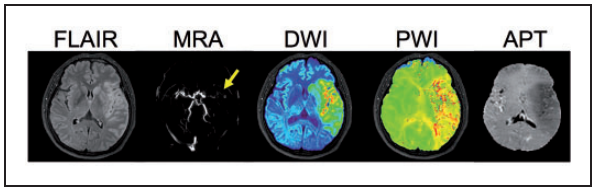

Figure 4. Multi-parameter MRI in an acute stroke patient with left MCA occlusion at 6 h 40 min after last seen normal. FLAIR (T2-weighted image with CSF suppression) image shows some early vasogenic edema outlining the cortex, while DWI hyperintensity shows a larger region with cytotoxic edema. The PWI (relative bolus transit time in this image) shows a large hypoperfusion region and the APT image shows a large area of reduced pH effect (hypointensity) that is larger than the hyperintense region on FLAIR and similar in size approximately to the ADC, but smaller than the area affected in PWI, suggesting minimal penumbral tissue but areas of benign oligemia. (Reproduced in part, with permission, from Heo HY et al. unpublished data).

doubt is fastest, it has the disadvantages of limited physiologic information and radiation exposure. On the other hand, while MRI scanners are more often being placed in close proximity to the emergency room, an MRI exam takes longer to set up (magnetic screening requirement) and care has to be taken with use of ferromagnetic materials (e.g. oxygen bottles). With respect to the appropriate physiological imaging parameters to be used for fast and easy image analysis in the clinic, a high priority is that they should preferably be the same, or very similar, in white matter and gray matter, which points to *MTT*, *OEF*, lactate, *pH*, PCr, ATP, and *ADC* (DWI). FLAIR images (T_2 hyperintensity based) can clearly outline ultimately infarcted tissue on both white and gray matter, but cannot distinguish old from new injuries, which can be accomplished with the FLAIR/DWI combination. At the moment, there are no proton MRI imaging modalities for ATP and PCr, although the latter is in principle possible with CEST MRI.[128] Lactate imaging can be done with spectroscopy (spectroscopic imaging) and may become faster in the future, but is currently to slow for whole-brain assessment. So this leaves *MTT, OEF*, *pH* and *ADC*. Of these, *MTT* and *OEF* are not specific for assigning a penumbra (Figure 1) as these parameters already change for flows corresponding to benign oligemia. So appropriate thresholds will have to be used. For *MTT* and *Tmax* or *TTP*, many manufacturers have their own software and numbers differ substantially between sites, complicating the standardization of thresholds. Also, the inner boundary of the CT penumbra is generally based on *MTT* combined with *CBV* or *CBF*, again bringing in the gray matter versus white matter issue. As such, it appears that MRI is theoretically most suitable, with *pH* imaging for the outer rim of the penumbra and *ADC* (DWI) imaging as the approximate inner rim as the most appropriate surrogate marker candidates. A good example of this potential is shown in the middle cerebral artery occlusion (MCAO) experiments on rats in Figure 3[121] and potential for application in humans is illustrated in Figure 4.

While the purpose for developing advanced MRI sequences has been to guide reperfusion therapies, it is entirely possible that such a methodology could be informative about other aspects of acute and chronic cerebrovascular disease. Identifying metabolically active tissue could help evaluate the success of reperfusion treatment and guide neuroprotective interventions or rehabilitation strategies. They are also expected to be very useful for drug development studies in the preclinical setting as well as the following trials. Finally, advanced physiologic imaging has potential value for studying cerebral ischemic evolution, both acute and chronic (e.g. for partial carotid occlusion or sickle cell disease) and maybe even for vascular dementia.

Conclusions

This review has traversed our understanding of the ischemic penumbra from its inception in animal models to its realization in human stroke. Clinically, visualization of the ischemic penumbra, while not currently employed in standard practice, holds the greatest potential for expanding our acute treatment options for this devastating disease. While rapid evaluation will always be integral to stroke care and non-contrast, CT/CTA is the currently accepted practice, imaging the ischemic penumbra offers the potential to treat patients who cannot be managed with time metrics alone. There remains a vital need for a concise imaging modality that can provide all of the necessary information to make informed clinical decisions. The ischemic penumbra evolves at the molecular level through a dynamic interaction between the available cerebral blood flow, the metabolic state of the tissue, and the duration of ischemia. Many methods of visualizing the ischemic penumbra have been employed, each with their distinct advantages and disadvantages. In the end, in the setting of acute stroke where time is of the essence, it is most important to have images that are easy to digest by the clinician to allow fast decision making. Images displaying parameters that differ between gray and white matter or for which thresholds change with the evolution of the stroke (*CBF*, *CBV*, *CMRO2*) are not as practical as those for which the physiology is immediately displayed (*OEF*, *pH*, DWI, *MTT*). While CT is fastest, MRI is unique in that it bridges the divide between accuracy and availability. It has already been demonstrated that MRI can be used

to rapidly triage acute stroke patients for treatment.[72] The American Heart Association (AHA) recommends that imaging occurs within 25 min of arrival, and that interpretation of imaging occurs within 45 min of arrival.[129] This leaves a 20-min window to acquire and interpret the images. A suitable imaging exam will need to meet this requirement. Based on current evidence, we conclude that a simple exam including *pH* imaging and DWI for the penumbra, *MTT* for perfusion analysis, MRA for vessel patency, and *T2**/SWI for hemorrhage should be achievable in the near future in about 10–15 min. Future trials including such a comprehensive fast MRI exam are needed to assess the potential benefit for these advanced imaging methods for patients that can currently not be treated, for assessing the effects of treatment, and for assessing the effect of neuroprotective strategies.

Funding

The author(s) disclosed receipt of the following financial support for the research, authorship, and/or publication of this article: This work was funded by NINDS Intramural Research Program, NIH (RL), P41EB015909 (PvZ), RO1NS083435 (JZ).

Declaration of conflicting interests

The author(s) declared the following potential conflicts of interest with respect to the research, authorship, and/or publication of this article: van Zijl and Zhou report grants from NIH. Knutsson has grants from the Swedish Research Council. In addition, van Zijl and Zhou have a patent on APT-weighted MRI for pH imaging with royalties paid by Philips. van Zijl also has a patent on VASO MRI for CBV imaging licensed to Philips. Leigh has no conflicts to report.

References

1. Pexman JH, Barber PA, Hill MD, et al. Use of the Alberta Stroke Program Early CT Score (ASPECTS) for assessing CT scans in patients with acute stroke. *AJNR Am J Neuroradiol* 2001; 22: 1534–1542.
2. Tissue plasminogen activator for acute ischemic stroke. The National Institute of Neurological Disorders and Stroke rt-PA Stroke Study Group. *N Engl J Med* 1995; 333: 1581–1587.
3. Saver JL, Fonarow GC, Smith EE, et al. Time to treatment with intravenous tissue plasminogen activator and outcome from acute ischemic stroke. *JAMA* 2013; 309: 2480–2488.
4. Demaerschalk BM, Kleindorfer DO, Adeoye OM, et al. Scientific rationale for the inclusion and exclusion criteria for intravenous alteplase in acute ischemic stroke: A statement for healthcare professionals from the American Heart Association/American Stroke Association. *Stroke* 2016; 47: 581–641.
5. Berkhemer OA, Fransen PS, Beumer D, et al. A randomized trial of intraarterial treatment for acute ischemic stroke. *N Engl J Med* 2015; 372: 11–20.
6. Goyal M, Demchuk AM, Menon BK, et al. Randomized assessment of rapid endovascular treatment of ischemic stroke. *N Engl J Med* 2015; 372: 1019–1030.
7. Campbell BC, Mitchell PJ, Kleinig TJ, et al. Endovascular therapy for ischemic stroke with perfusion-imaging selection. *N Engl J Med* 2015; 372: 1009–1018.
8. Saver JL, Goyal M, Bonafe A, et al. Stent-retriever thrombectomy after Intravenous t-PA vs. t-PA alone in stroke. *N Engl J Med* 2015; 372: 2285–2295.
9. Powers WJ, Derdeyn CP, Biller J, et al. 2015 AHA/ASA focused update of the 2013 guidelines for the early management of patients with acute ischemic stroke regarding endovascular treatment: A guideline for healthcare professionals from the American Heart Association/American Stroke Association. *Stroke* 2015; 46: 3020–3035.
10. Mozaffarian D, Benjamin EJ, Go AS, et al. Heart disease and stroke statistics – 2015 update: A report from the American Heart Association. *Circulation* 2015; 131: e29–e322.
11. Baron JC. Mapping the ischaemic penumbra with PET: Implications for acute stroke treatment. *Cerebrovasc Dis* 1999; 9: 193–201.
12. Baron JC. Mapping the ischaemic penumbra with PET: A new approach. *Brain* 2001; 124: 2–4.
13. Baron JC. How healthy is the acutely reperfused ischemic penumbra? *Cerebrovasc Dis* 2005; 20(Suppl 2): 25–31.
14. Baron JC. Recent advances in mesoscopic-scale imaging in animal models of ischemic stroke. *Curr Opin Neurol* 2016; 29: 104–111.
15. Dani KA and Warach S. Metabolic imaging of ischemic stroke: the present and future. *AJNR Am J Neuroradiol* 2014; 35: S37–S43.
16. Heiss WD. The concept of the penumbra: Can it be translated to stroke management? *Int J Stroke* 2010; 5: 290–295.
17. Hossmann KA. Pathophysiological basis of translational stroke research. *Folia Neuropathol* 2009; 47: 213–227.
18. Mlynash M, Lansberg MG, De Silva DA, et al. Refining the definition of the malignant profile: Insights from the DEFUSE-EPITHET pooled data set. *Stroke* 2011; 42: 1270–1275.
19. Leigh R, Christensen S, Campbell BC, et al. Pretreatment blood-brain barrier disruption and post-endovascular intracranial hemorrhage. *Neurology* 2016; 87: 263–269.
20. Astrup J, Symon L, Branston N, et al. Thresholds of cerebral ischemia. In: Schmiedek P (ed.) *Microsurgery for stroke*. Berlin: Springer, 1976, pp.16–21.
21. Astrup J, Siesjo BK and Symon L. Thresholds in cerebral ischemia – the ischemic penumbra. *Stroke* 1981; 12: 723–725.
22. Baron JC, Bousser MG, Rey A, et al. Reversal of focal "misery-perfusion syndrome" by extra-intracranial arterial bypass in hemodynamic cerebral ischemia. A case study with 15O positron emission tomography. *Stroke* 1981; 12: 454–459.
23. Hossmann KA. Viability thresholds and the penumbra of focal ischemia. *Ann Neurol* 1994; 36: 557–565.

24. Heiss WD. Ischemic penumbra: Evidence from functional imaging in man. *J Cereb Blood Flow Metab* 2000; 20: 1276–1293.
25. Baron JC. Perfusion thresholds in human cerebral ischemia: Historical perspective and therapeutic implications. *Cerebrovasc Dis* 2001; 11(Suppl 1): 2–8.
26. Paciaroni M, Caso V and Agnelli G. The concept of ischemic penumbra in acute stroke and therapeutic opportunities. *Eur Neurol* 2009; 61: 321–330.
27. Kohno K, Hoehn-Berlage M, Mies G, et al. Relationship between diffusion-weighted MR images, cerebral blood flow, and energy state in experimental brain infarction. *Magn Reson Imaging* 1995; 13: 73–80.
28. Powers WJ. Cerebral hemodynamics in ischemic cerebrovascular disease. *Ann Neurol* 1991; 29: 231–240.
29. Iadecola C. Neurovascular regulation in the normal brain and in Alzheimer's disease. *Nat Rev Neurosci* 2004; 5: 347–360.
30. Peppiatt CM, Howarth C, Mobbs P, et al. Bidirectional control of CNS capillary diameter by pericytes. *Nature* 2006; 443: 700–704.
31. Meier P and Zierler KL. On the theory of the indicator-dilution method for measurement of blood flow and volume. *J Appl Physiol* 1954; 6: 731–744.
32. Mies G, Auer LM, Ebhardt G, et al. Flow and neuronal density in tissue surrounding chronic infarction. *Stroke* 1983; 14: 22–27.
33. Paschen W, Mies G and Hossmann KA. Threshold relationship between cerebral blood flow, glucose utilization, and energy metabolites during development of stroke in gerbils. *Exp Neurol* 1992; 117: 325–333.
34. Allen K, Busza AL, Crockard HA, et al. Acute cerebral ischaemia: Concurrent changes in cerebral blood flow, energy metabolites, pH, and lactate measured with hydrogen clearance and 31P and 1H nuclear magnetic resonance spectroscopy. III. Changes following ischaemia. *J Cereb Blood Flow Metab* 1988; 8: 816–821.
35. Crockard HA, Gadian DG, Frackowiak RS, et al. Acute cerebral ischaemia: Concurrent changes in cerebral blood flow, energy metabolites, pH, and lactate measured with hydrogen clearance and 31P and 1H nuclear magnetic resonance spectroscopy. II. Changes during ischaemia. *J Cereb Blood Flow Metab* 1987; 7: 394–402.
36. Naritomi H, Sasaki M, Kanashiro M, et al. Flow thresholds for cerebral energy disturbance and Na + pump failure as studied by in vivo 31P and 23Na nuclear magnetic resonance spectroscopy. *J Cereb Blood Flow Metab* 1988; 8: 16–23.
37. Astrup J, Symon L, Branston NM, et al. Cortical evoked potential and extracellular K + and H + at critical levels of brain ischemia. *Stroke* 1977; 8: 51–57.
38. Taylor JM, Zhu XH, et al. Dynamic correlations between hemodynamic, metabolic, and neuronal responses to acute whole-brain ischemia. *NMR Biomed* 2015; 28: 1357–1365.
39. Symon L, Branston NM, Strong AJ, et al. The concepts of thresholds of ischaemia in relation to brain structure and function. *J Clin Pathol Suppl* 1977; 11: 149–154.
40. Jones TH, Morawetz RB, Crowell RM, et al. Thresholds of focal cerebral ischemia in awake monkeys. *J Neurosurg* 1981; 54: 773–782.
41. Garcia JH, Mitchem HL, Briggs L, et al. Transient focal ischemia in subhuman primates. Neuronal injury as a function of local cerebral blood flow. *J Neuropathol Exp Neurol* 1983; 42: 44–60.
42. Simon JE, Bristow MS, Lu H, et al. A novel method to derive separate gray and white matter cerebral blood flow measures from MR imaging of acute ischemic stroke patients. *J Cereb Blood Flow Metab* 2005; 25: 1236–1243.
43. Bristow MS, Simon JE, Brown RA, et al. MR perfusion and diffusion in acute ischemic stroke: human gray and white matter have different thresholds for infarction. *J Cereb Blood Flow Metab* 2005; 25: 1280–1287.
44. van Gelderen P, de Vleeschouwer MH, DesPres D, et al. Water diffusion and acute stroke. *Magn Reson Med* 1994; 31: 154–163.
45. Ulug AM, Beauchamp N Jr, Bryan RN, et al. Absolute quantitation of diffusion constants in human stroke. *Stroke* 1997; 28: 483–490.
46. Latour LL, Hasegawa Y, Formato JE, et al. Spreading waves of decreased diffusion coefficient after cortical stimulation in the rat brain. *Magn Reson Med* 1994; 32: 189–198.
47. Els T, Rother J, Beaulieu C, et al. Hyperglycemia delays terminal depolarization and enhances repolarization after peri-infarct spreading depression as measured by serial diffusion MR mapping. *J Cereb Blood Flow Metab* 1997; 17: 591–595.
48. Grohn OH, Lukkarinen JA, Oja JM, et al. Noninvasive detection of cerebral hypoperfusion and reversible ischemia from reductions in the magnetic resonance imaging relaxation time, T2. *J Cereb Blood Flow Metab* 1998; 18: 911–920.
49. van Zijl PC, Eleff SM, Ulatowski JA, et al. Quantitative assessment of blood flow, blood volume and blood oxygenation effects in functional magnetic resonance imaging. *Nat Med* 1998; 4: 159–167.
50. Heiss WD, Graf R, Fujita T, et al. Early detection of irreversibly damaged ischemic tissue by flumazenil positron emission tomography in cats. *Stroke* 1997; 28: 2045–2051; discussion 51–52.
51. Sakamoto Y, Kimura K, Shibazaki K, et al. Early ischaemic diffusion lesion reduction in patients treated with intravenous tissue plasminogen activator: Infrequent, but significantly associated with recanalization. *Int J Stroke* 2013; 8: 321–326.
52. Labeyrie MA, Turc G, Hess A, et al. Diffusion lesion reversal after thrombolysis: A MR correlate of early neurological improvement. *Stroke* 2012; 43: 2986–2991.
53. Loh PS, Butcher KS, Parsons MW, et al. Apparent diffusion coefficient thresholds do not predict the response to acute stroke thrombolysis. *Stroke* 2005; 36: 2626–2631.
54. Olivot JM, Mlynash M, Thijs VN, et al. Relationships between cerebral perfusion and reversibility of acute diffusion lesions in DEFUSE. Insights from RADAR. *Stroke* 2009; 40: 1692–1697.

55. Fiehler J, Foth M, Kucinski T, et al. Severe ADC decreases do not predict irreversible tissue damage in humans. *Stroke* 2002; 33: 79–86.
56. Fiehler J, Knudsen K, Kucinski T, et al. Predictors of apparent diffusion coefficient normalization in stroke patients. *Stroke* 2004; 35: 514–519.
57. Back T, Hoehn-Berlage M, Kohno K, et al. Diffusion nuclear magnetic resonance imaging in experimental stroke. Correlation with cerebral metabolites. *Stroke* 1994; 25: 494–500.
58. Moseley ME, Cohen Y, Mintorovitch J, et al. Early detection of regional cerebral ischemia in cats: Comparison of diffusion- and T2-weighted MRI and spectroscopy. *Magn Reson Med* 1990; 14: 330–346.
59. Warach S, Chien D, Li W, et al. Fast magnetic resonance diffusion-weighted imaging of acute human stroke. *Neurology* 1992; 42: 1717–1723.
60. Kidwell CS, Alger JR and Saver JL. Beyond mismatch: Evolving paradigms in imaging the ischemic penumbra with multimodal magnetic resonance imaging. *Stroke* 2003; 34: 2729–2735.
61. Mintorovitch J, Yang GY, Shimizu H, et al. Diffusion-weighted magnetic resonance imaging of acute focal cerebral ischemia: Comparison of signal intensity with changes in brain water and Na+,K(+)-ATPase activity. *J Cereb Blood Flow Metab* 1994; 14: 332–336.
62. Davis D, Ulatowski J, Eleff S, et al. Rapid monitoring of changes in water diffusion coefficients during reversible ischemia in cat and rat brain. *Magn Reson Med* 1994; 31: 454–460.
63. Rother J, de Crespigny AJ, D'Arceuil H, et al. Recovery of apparent diffusion coefficient after ischemia-induced spreading depression relates to cerebral perfusion gradient. *Stroke* 1996; 27: 980–986.
64. Campbell BC, Purushotham A, Christensen S, et al. The infarct core is well represented by the acute diffusion lesion: Sustained reversal is infrequent. *J Cereb Blood Flow Metab* 2012; 32: 50–56.
65. Wheeler HM, Mlynash M, Inoue M, et al. Early diffusion-weighted imaging and perfusion-weighted imaging lesion volumes forecast final infarct size in DEFUSE 2. *Stroke* 2013; 44: 681–685.
66. Baron JC, Bousser MG, Comar D, et al. Noninvasive tomographic study of cerebral blood flow and oxygen metabolism in vivo. Potentials, limitations, and clinical applications in cerebral ischemic disorders. *Eur Neurol* 1981; 20: 273–284.
67. Guadagno JV, Donnan GA, Markus R, et al. Imaging the ischaemic penumbra. *Curr Opin Neurol* 2004; 17: 61–67.
68. Heit JJ and Wintermark M. Perfusion computed tomography for the evaluation of acute ischemic stroke: strengths and pitfalls. *Stroke* 2016; 47: 1153–1158.
69. Finelli DA, Hopkins AL, Selman WR, et al. Evaluation of experimental early acute cerebral ischemia before the development of edema: Use of dynamic, contrast-enhanced and diffusion-weighted MR scanning. *Magn Reson Med* 1992; 27: 189–197.
70. Hamberg LM, Macfarlane R, Tasdemiroglu E, et al. Measurement of cerebrovascular changes in cats after transient ischemia using dynamic magnetic resonance imaging. *Stroke* 1993; 24: 444–450; discussion 50–51.
71. Schlaug G, Benfield A, Baird AE, et al. The ischemic penumbra: operationally defined by diffusion and perfusion MRI. *Neurology* 1999; 53: 1528–1537.
72. Shah S, Luby M, Poole K, et al. Screening with MRI for accurate and rapid stroke treatment: SMART. *Neurology* 2015; 84: 2438–2444.
73. Wendland MF, White DL, Aicher KP, et al. Detection with echo-planar MR imaging of transit of susceptibility contrast medium in a rat model of regional brain ischemia. *J Magn Reson Imaging* 1991; 1: 285–292.
74. Weisskoff RM, Chesler D, Boxerman JL, et al. Pitfalls in MR measurement of tissue blood flow with intravascular tracers: Which mean transit time? *Magn Reson Med* 1993; 29: 553–558.
75. Wang DJ, Alger JR, Qiao JX, et al. Multi-delay multi-parametric arterial spin-labeled perfusion MRI in acute ischemic stroke – Comparison with dynamic susceptibility contrast enhanced perfusion imaging. *Neuroimage Clinical* 2013; 3: 1–7.
76. Villringer A, Rosen BR, Belliveau JW, et al. Dynamic imaging with lanthanide chelates in normal brain: contrast due to magnetic susceptibility effects. *Magn Reson Med* 1988; 6: 164–174.
77. Albers GW, Thijs VN, Wechsler L, et al. Magnetic resonance imaging profiles predict clinical response to early reperfusion: The diffusion and perfusion imaging evaluation for understanding stroke evolution (DEFUSE) study. *Ann Neurol* 2006; 60: 508–517.
78. Davis SM, Donnan GA, Parsons MW, et al. Effects of alteplase beyond 3 h after stroke in the Echoplanar Imaging Thrombolytic Evaluation Trial (EPITHET): A placebo-controlled randomised trial. *Lancet Neurol* 2008; 7: 299–309.
79. Lansberg MG, Lee J, Christensen S, et al. RAPID automated patient selection for reperfusion therapy: A pooled analysis of the Echoplanar Imaging Thrombolytic Evaluation Trial (EPITHET) and the Diffusion and Perfusion Imaging Evaluation for Understanding Stroke Evolution (DEFUSE) Study. *Stroke* 2011; 42: 1608–1614.
80. Olivot JM, Mlynash M, Thijs VN, et al. Optimal Tmax threshold for predicting penumbral tissue in acute stroke. *Stroke* 2009; 40: 469–475.
81. Knutsson L, Stahlberg F and Wirestam R. Absolute quantification of perfusion using dynamic susceptibility contrast MRI: Pitfalls and possibilities. *MAGMA* 2010; 23: 1–21.
82. Knutsson L and Kjolby B. *Cerebral perfusion imaging*. *Oxford textbooks of neuroimaging*. Oxford: Oxford University Press, 2015.
83. Thijs VN, Somford DM, Bammer R, et al. Influence of arterial input function on hypoperfusion volumes measured with perfusion-weighted imaging. *Stroke* 2004; 35: 94–98.
84. Calamante F, Christensen S, Desmond PM, et al. The physiological significance of the time-to-maximum (Tmax) parameter in perfusion MRI. *Stroke* 2010; 41: 1169–1174.

85. Zaro-Weber O, Moeller-Hartmann W, Heiss WD, et al. Maps of time to maximum and time to peak for mismatch definition in clinical stroke studies validated with positron emission tomography. *Stroke* 2010; 41: 2817–2821.
86. Kidwell CS, Saver JL, Mattiello J, et al. Thrombolytic reversal of acute human cerebral ischemic injury shown by diffusion/perfusion magnetic resonance imaging. *Ann Neurol* 2000; 47: 462–469.
87. Lansberg MG, Straka M, Kemp S, et al. MRI profile and response to endovascular reperfusion after stroke (DEFUSE 2): A prospective cohort study. *Lancet Neurol* 2012; 11: 860–867.
88. Wintermark M, Flanders AE, Velthuis B, et al. Perfusion-CT assessment of infarct core and penumbra: Receiver operating characteristic curve analysis in 130 patients suspected of acute hemispheric stroke. *Stroke* 2006; 37: 979–985.
89. Campbell BC, Christensen S, Levi CR, et al. Cerebral blood flow is the optimal CT perfusion parameter for assessing infarct core. *Stroke* 2011; 42: 3435–3440.
90. Bivard A, Levi C, Spratt N, et al. Perfusion CT in acute stroke: A comprehensive analysis of infarct and penumbra. *Radiology* 2013; 267: 543–550.
91. Schaefer PW, Souza L, Kamalian S, et al. Limited reliability of computed tomographic perfusion acute infarct volume measurements compared with diffusion-weighted imaging in anterior circulation stroke. *Stroke* 2015; 46: 419–424.
92. Campbell BC, Christensen S, Levi CR, et al. Comparison of computed tomography perfusion and magnetic resonance imaging perfusion-diffusion mismatch in ischemic stroke. *Stroke* 2012; 43: 2648–2653.
93. Kudo K, Christensen S, Sasaki M, et al. Accuracy and reliability assessment of CT and MR perfusion analysis software using a digital phantom. *Radiology* 2013; 267: 201–211.
94. Markus R, Donnan GA, Kazui S, et al. Statistical parametric mapping of hypoxic tissue identified by [(18)F]fluoromisonidazole and positron emission tomography following acute ischemic stroke. *Neuroimage* 2002; 16: 425–433.
95. Markus R, Reutens DC, Kazui S, et al. Topography and temporal evolution of hypoxic viable tissue identified by 18F-fluoromisonidazole positron emission tomography in humans after ischemic stroke. *Stroke* 2003; 34: 2646–2652.
96. Markus R, Donnan G, Kazui S, et al. Penumbral topography in human stroke: Methodology and validation of the 'Penumbragram'. *Neuroimage* 2004; 21: 1252–1259.
97. Read SJ, Hirano T, Abbott DF, et al. Identifying hypoxic tissue after acute ischemic stroke using PET and 18F-fluoromisonidazole. *Neurology* 1998; 51: 1617–1621.
98. Takasawa M, Beech JS, Fryer TD, et al. Imaging of brain hypoxia in permanent and temporary middle cerebral artery occlusion in the rat using 18F-fluoromisonidazole and positron emission tomography: A pilot study. *J Cereb Blood Flow Metab* 2007; 27: 679–689.
99. Markus R, Reutens DC, Kazui S, et al. Hypoxic tissue in ischaemic stroke: Persistence and clinical consequences of spontaneous survival. *Brain* 2004; 127: 1427–1436.
100. Heiss WD, Sobesky J and Hesselmann V. Identifying thresholds for penumbra and irreversible tissue damage. *Stroke* 2004; 35: 2671–2674.
101. Lu H, Xu F, Grgac K, et al. Calibration and validation of TRUST MRI for the estimation of cerebral blood oxygenation. *Magn Reson Med* 2012; 67: 42–49.
102. Oja JM, Gillen JS, Kauppinen RA, et al. Determination of oxygen extraction ratios by magnetic resonance imaging. *J Cereb Blood Flow Metab* 1999; 19: 1289–1295.
103. Qin Q, Grgac K and van Zijl PC. Determination of whole-brain oxygen extraction fractions by fast measurement of blood T(2) in the jugular vein. *Magn Reson Med* 2011; 65: 471–479.
104. Wright GA, Hu BS and Macovski A. 1991 I.I. Rabi award. Estimating oxygen saturation of blood in vivo with MR imaging at 1.5 T. *J Magn Reson Imaging* 1991; 1: 275–283.
105. Barhoum S, Rodgers ZB, Langham M, et al. Comparison of MRI methods for measuring whole-brain venous oxygen saturation. *Magn Reson Med* 2015; 73: 2122–2128.
106. Fernandez-Seara MA, Techawiboonwong A, Detre JA, et al. MR susceptometry for measuring global brain oxygen extraction. *Magn Reson Med* 2006; 55: 967–973.
107. Fujima N, Kudo K, Terae S, et al. Non-invasive measurement of oxygen saturation in the spinal vein using SWI: Quantitative evaluation under conditions of physiological and caffeine load. *Neuroimage* 2011; 54: 344–349.
108. Langham MC, Magland JF, Floyd TF, et al. Retrospective correction for induced magnetic field inhomogeneity in measurements of large-vessel hemoglobin oxygen saturation by MR susceptometry. *Magn Reson Med* 2009; 61: 626–633.
109. Rodgers ZB, Detre JA and Wehrli FW. MRI-based methods for quantification of the cerebral metabolic rate of oxygen. *J Cereb Blood Flow Metab* 2016; 36: 1165–1185.
110. An H and Lin W. Cerebral oxygen extraction fraction and cerebral venous blood volume measurements using MRI: effects of magnetic field variation. *Magn Reson Med* 2002; 47: 958–966.
111. An H, Lin W, Celik A and Lee YZ. Quantitative measurements of cerebral metabolic rate of oxygen utilization using MRI: A volunteer study. *NMR Biomed* 2001; 14: 441–447.
112. An H, Liu Q, Chen Y, et al. Evaluation of MR-derived cerebral oxygen metabolic index in experimental hyperoxic hypercapnia, hypoxia, and ischemia. *Stroke* 2009; 40: 2165–2172.
113. Yablonskiy DA and Haacke EM. Theory of NMR signal behavior in magnetically inhomogeneous tissues: The static dephasing regime. *Magn Reson Med* 1994; 32: 749–763.
114. Lin W, An H, Ford AL, et al. MR imaging of oxygen extraction and neurovascular coupling. *Stroke* 2013; 44: S61–S64.

115. Barker PB, Gillard JH, van Zijl PC, et al. Acute stroke: Evaluation with serial proton MR spectroscopic imaging. *Radiology* 1994; 192: 723–732.
116. Mori S, Eleff SM, Pilatus U, et al. Proton NMR spectroscopy of solvent-saturable resonances: A new approach to study pH effects in situ. *Magn Reson Med* 1998; 40: 36–42.
117. Liepinsh E and Otting G. Proton exchange rates from amino acid side chains – implications for image contrast. *Magn Reson Med* 1996; 35: 30–42.
118. Ward KM, Aletras AH and Balaban RS. A new class of contrast agents for MRI based on proton chemical exchange dependent saturation transfer (CEST). *J Magn Reson* 2000; 143: 79–87.
119. Zhou J and van Zijl PC. Chemical exchange saturation transfer imaging and spectroscopy. *Progr NMR Spectr* 2006; 48: 109–136.
120. Zhou J, Payen JF, Wilson DA, et al. Using the amide proton signals of intracellular proteins and peptides to detect pH effects in MRI. *Nat Med* 2003; 9: 1085–1090.
121. Sun PZ, Zhou J, Sun W, et al. Detection of the ischemic penumbra using pH-weighted MRI. *J Cereb Blood Flow Metab* 2007; 27: 1129–1136.
122. Zhou JY and van Zijl PCM. Defining an acidosis-based ischemic penumbra from pH-weighted MRI. *Transl Stroke Res* 2012; 3: 76–83.
123. Ghosh N, Yuan X, Turenius CI, et al. Automated core-penumbra quantification in neonatal ischemic brain injury. *J Cereb Blood Flow Metab* 2012; 32: 2161–2170.
124. Popp A, Jaenisch N, Witte OW, et al. Identification of ischemic regions in a rat model of stroke. *PloS One* 2009; 4: e4764.
125. Hilger T, Blunk JA, Hoehn M, et al. Characterization of a novel chronic photothrombotic ring stroke model in rats by magnetic resonance imaging, biochemical imaging, and histology. *J Cereb Blood Flow Metab* 2004; 24: 789–797.
126. Harston GW, Tee YK, Blockley N, et al. Identifying the ischaemic penumbra using pH-weighted magnetic resonance imaging. *Brain* 2015; 138: 36–42.
127. Tietze A, Blicher J, Mikkelsen IK, et al. Assessment of ischemic penumbra in patients with hyperacute stroke using amide proton transfer (APT) chemical exchange saturation transfer (CEST) MRI. *NMR Biomed* 2014; 27: 163–174.
128. Haris M, Nanga RP, Singh A, et al. Exchange rates of creatine kinase metabolites: Feasibility of imaging creatine by chemical exchange saturation transfer MRI. *NMR Biomed* 2012; 25: 1305–1309.
129. Fonarow GC, Smith EE, Saver JL, et al. Improving door-to-needle times in acute ischemic stroke: The design and rationale for the American Heart Association/American Stroke Association's Target: Stroke initiative. *Stroke* 2011; 42: 2983–2989.
130. Cheng AL, Batool S, McCreary CR, et al. Susceptibility-weighted imaging is more reliable than T2*-weighted gradient-recalled echo MRI for detecting microbleeds. *Stroke* 2013; 44: 2782–2786.
131. Wang M, Hong X, Chang CF, et al. Simultaneous detection and separation of hyperacute intracerebral hemorrhage and cerebral ischemia using amide proton transfer MRI. *Magn Reson Med* 2015; 74(1): 42–50.
132. Lu H, Hua J and van Zijl PC. Noninvasive functional imaging of cerebral blood volume with vascular-space-occupancy (VASO) MRI. *NMR Biomed* 2013; 26: 932–948.
133. Hua J, Qin Q, Donahue MJ, et al. Inflow-based vascular-space-occupancy (iVASO) MRI. *Magn Reson Med* 2011; 66: 40–56.
134. Hartkamp NS, van Osch MJ, Kappelle J, et al. Arterial spin labeling magnetic resonance perfusion imaging in cerebral ischemia. *Curr Opin Neurol* 2014; 27: 42–53.